Charge extraction from colloidal inorganic nanocrystals

Szendrei, Krisztina

Chapter 5

Exploring the origin of the temperature dependent behavior of PbS solar cells

Abstract

This final chapter focuses on the temperature dependent behavior of PbS solar cells. We seek to explain the peculiar temperature dependence of physical parameters characterizing the PbS solar cells. Via low temperature absorption and photoluminescence (PL) measurements, we will demonstrate that the optical properties of PbS thin films before and after benzenedithiol (BDT) treatment exhibit very distinct behavior. After BDT treatment both the absorption and PL of the PbS NCs are shifted to lower energies, indicating the occurrence of wave function overlap between adjacent NCs. The PL of the thin films composed of PbS NCs surrounded by original oleic acid (OA) ligands shows red-shift and increase of the signal with decreasing temperature. After BDT treatment, the PbS thin films exhibit unusual properties, such as decrease of the PL signal and irregular shape of the spectra, which could be attributed to the increased probability of nonradiative recombination at lower temperatures.[*]

[*] K. Szendrei, M. Speirs, D. Jarzab, M. Manca, O. V. Mikhnenko, M. Yarema, W. Heiss, M. A. Loi, *manuscript in preparation*

5.1 Introduction

The optical properties of semiconductor nanocrystals (NCs) exhibit strong size dependence (Figure 1.4) due to the quantum confinement of the electronic wave functions. Therefore they are considered to be very promising candidates for optoelectronic applications.[1,2] In particular, PbX (X = S, Se) NCs have emerged as solution processable building blocks for device active layers, since they can access a greater portion of the near-infrared part of the solar spectrum, contrary to most of the organic polymers.[3,4] Besides the size, the shape of the NCs and the nature of the stabilizer ligands can also have large effects on the optical properties and the device performance.[1,5-8]

As it has been mentioned in the previous chapter, charge transport in surface modified PbX NC thin films is not yet well understood. There are several studies focusing on transport properties of surface modified PbX NC thin films used as active layers in field-effect transistors (FET) and solar cells.[4,9-12] The active layer is generally prepared by spin-coating of PbX NCs (for more details see Chapter 4) followed by the solid state ligand exchange using different short molecules such as thiols and amines.[13-18] As a result, the NCs form a disordered system of localized, but coupled electronic states with site energies distributed in a Gaussian manner.[11] Few theories have been developed to try to explain charge separation and charge conduction in these NC-based devices. Choi *et al.* suggested that charge separation most probably occurs via tunneling through a potential barrier without the aid of an external bias of potential gradient.[16] On the other hand, the free carrier transport following the charge separation is still to be considered. However, FET studies[11,13,19] suggest that long range charge transport in NC solids occurs via a series of incoherent tunneling transitions between adjacent NCs, namely by nearest-neighbor hopping. This means that thousands of individual hops are required for the free carriers to reach the electrodes. In contrast, Tang *et al.*[20] and Luther *et al.*[4] reported on a different mechanism in PbX Schottky solar cells, where the electron-hole pairs are separated by the built-in field followed by diffusion and drift of electrons and holes to the corresponding electrodes under the influence of the electric field. Due to uncertainties in the nature of the mechanism of the device performance, further experimental and theoretical investigations are required for deeper understanding. Low temperature studies on cross-linked PbX NC thin films could provide extra important information to gain insight into the working mechanisms.

The temperature dependent optical properties of NCs, stabilized by insulating organic ligands, have been extensively investigated in thin films of NCs providing necessary basics for device applications.[21-27] In general, it has been shown that

reduced temperature can produce characteristic changes in the absorption and PL spectra, such as increasing the intensity of absorption and PL bands, reduction of the full width half maximum (FWHM), changes in the number of bands and shifts of the absorption and PL maxima. The increase in the intensity of the PL spectra originates from the fact that at lower temperatures the number of electron-phonon interactions is reduced, which leads to an increased probability of radiative transitions. In PbS NC thin films, the shift of the spectral maxima can be explained by considering the thermal expansion of the NCs`s bandgap (E_g). PbS has a positive temperature coefficient (dE_g/dT) which is unique among binary compound semiconductors. The temperature dependence of the E_g originates from the change of the lattice constant (the edge distance between Pb ions) and of the electron-phonon interactions with temperature. This effect has already been shown in several studies on PbS NC-based thin films.[21,22,28]

Nevertheless, to the best of our knowledge, there are no reports in literature on the temperature dependent absorption, PL and *J-V* characteristics of post-deposition ligand exchanged PbS NCs thin films. Therefore, in this chapter we introduce the temperature dependence study of electrical and optical properties of PbS NCs thin films. These low temperature measurements provide a better understanding of the device working mechanism and the physics of the cross-linked NC arrays.

5.2 Results and discussion

5.2.1 Temperature dependence of J-V characteristics

As was mentioned in Chapter 4, PbS NC solar cells were fabricated by spin coating PbS NCs (with a bandgap of 1.1 eV) stabilized by insulating oleic acid (OA) ligands onto ITO patterned glass. The PbS NCs were treated by benzenedithiol (BDT) to remove the insulating OA ligands and improve the charge transport in the PbS NC layer. The devices were completed by evaporation of 1 nm LiF and 100 nm Al on top of the active layer. To extract more information, the temperature dependent *J-V* characteristics of surface modified PbS NC solar cells were measured under AM 1.5 illumination and in dark (Figure 5.1 and inset).

Figure 5.1 shows the obtained *J-V* characteristics under illumination at various temperatures. As can be seen, the overall effect of the temperature on the device efficiency originates from the temperature dependence of V_{oc} and J_{sc}. The net effect is that V_{oc} increases and J_{sc} decreases with decreasing temperature, while the *FF* remains approximately constant. A similar effect can be observed for Si solar cells[29]; however, the decrease of J_{sc} is much smaller, which is generally due to the decreasing number of thermally generated carriers in the cell.

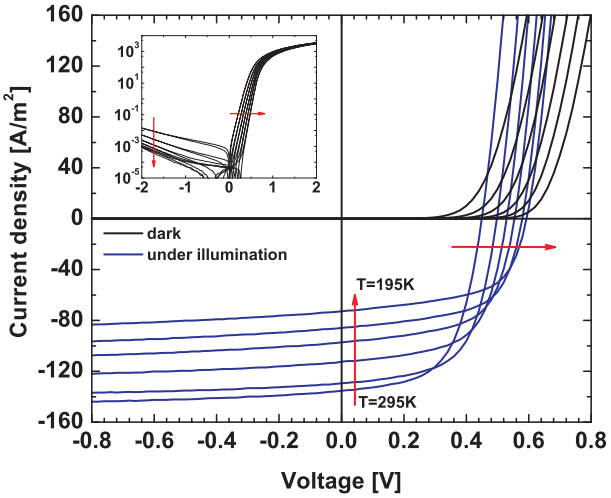

Figure 5.1 *J-V* characteristics of PbS NC solar cells under illumination from 293K to 195K. Inset shows the *J-V* characteristics on a logarithmic scale in dark.

In organic solar cells, losses in the *FF* also contribute to the decrease in the device efficiency besides the decrease of J_{sc}, owing to the reduced carrier mobilities at lower temperatures.[30,31]

The *J-V* characteristics of a Schottky solar cell under illumination can be expressed as[32]

$$J = J_0\left[\exp\left(\frac{qV}{nkT}\right)-1\right]-J_{ph} \qquad \text{Eq. 5.1.}$$

where J is the output current density, J_o is the reverse saturation current density, q is the elementary charge, V is the voltage across the cell, n is the ideality factor, k is the Boltzmann constant, T is the temperature and J_{ph} is the generated photocurrent density. At open circuit voltage (V_{oc}) the output current density $J=0$, therefore Eq.5.1. can be simplified and the V_{oc} can be expressed as

$$V_{oc} = \frac{nkT}{q}\ln\left(\frac{J_{ph}}{J_0}\right) \qquad \text{Eq.5.2.}$$

The temperature affects J (Eq. 5.1.) directly by means of the exponential term and indirectly via J_o. Clearly, a decrease in T increases the value of the exponent in Eq.5.1., while a reduction of T results in lower values of J_o, which will be shown later on (Figure 5.3 (b)). The net effect will be to increase V_{oc} with decreasing temperature. The reduction in J_{sc} of PbS NC solar cells with decreasing temperature is much more pronounced than in Si solar cells. It seems that the

number of generated carriers is drastically decreasing from 295K to 195K which could be due to an increase of carrier trapping by surface defects.

In contrast, the *FF* of the PbS NC devices stays approximately constant, as can be seen in Figure 5.2, where the *FF* is plotted together with the other characteristic parameters against the temperature.

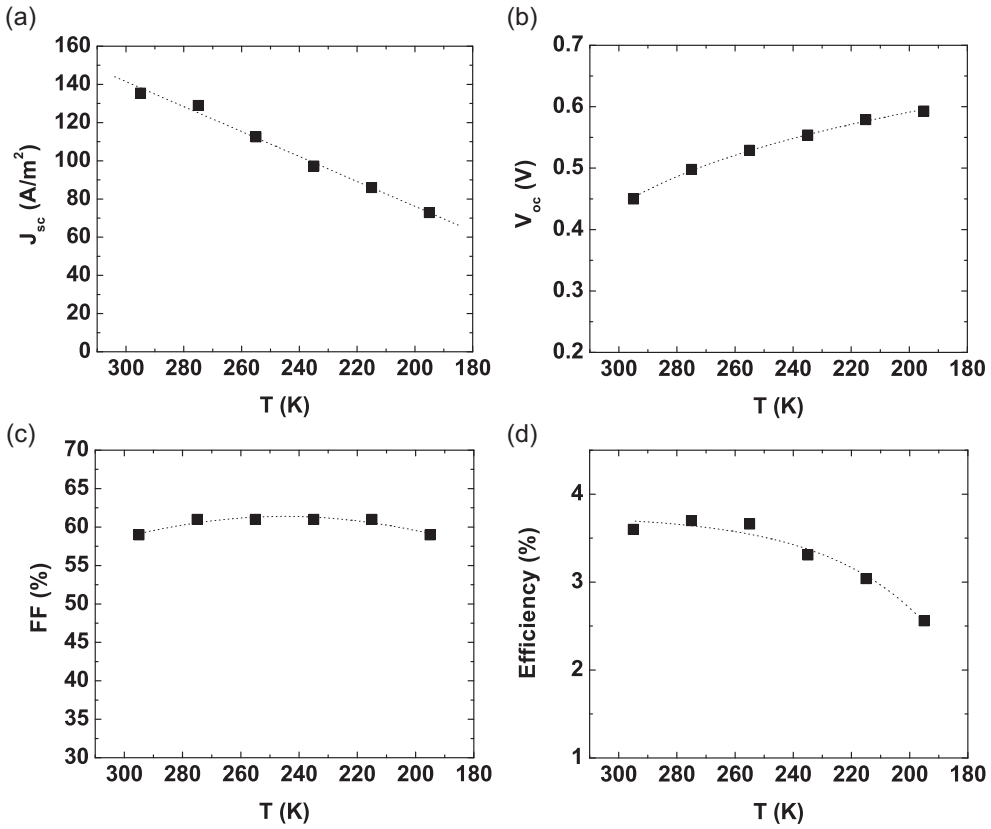

Figure 5.2 Temperature dependence of characteristic device parameters (J_{sc}, V_{oc}, *FF* and *efficiency*).

In general, it can be concluded, that the device efficiency slightly increases when the T is decreased from 293K to 255K, since the increase in V_{oc} is larger than the decrease in J_{sc}. However, below 255K the decrease in J_{sc} becomes dominating and the efficiency starts to decrease (Figure 5.2 d)).

The temperature dependence of the V_{oc} of the PbS solar cells can be analytically modeled by using the extracted values of the J_0 at different temperatures. The values of the J_0 cannot be directly measured, but they can be determined from the temperature dependent *J-V* characteristics of the solar cells measured in the dark (Figure 5.3 a)).

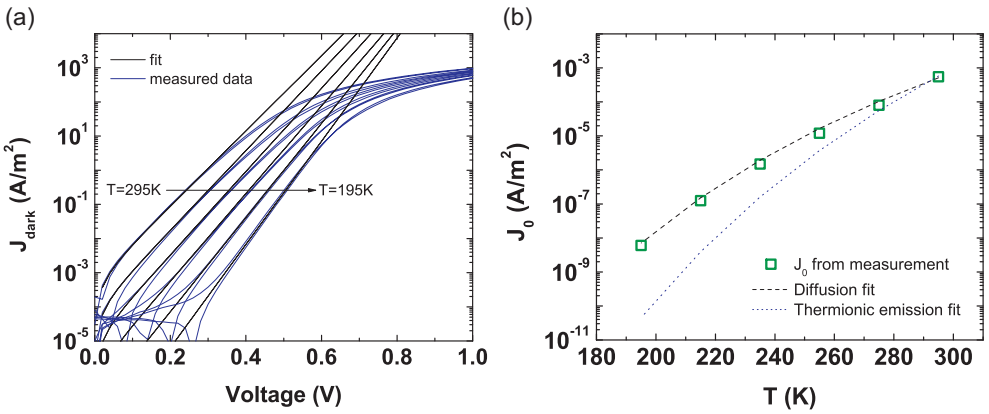

Figure 5.3 a) Dark *J-V* characteristics of PbS NC solar cells and b) temperature dependence of the J_0 modeled by using diffusion and thermionic emission theory.

By fitting the exponential part of the *J-V* characteristics to the Shockley diode equation (Eq. 5.3.), the two fit parameters J_0 and n can be determined[32]:

$$J = J_0\left[\exp\left(\frac{qV}{nkT}\right)-1\right] \qquad \text{Eq.5.3.}$$

The obtained saturation current density J_0 as a function of temperature is plotted in Figure 5.3 b) and it can conventionally be modeled within two theories.

The first theory is the so-called thermionic emission theory. This theory assumes that carriers with energy larger than the barrier height (ϕ_B) can only contribute to the current flow and the shape of the barrier profile is neglected. The current density can be expressed as[32]

$$J = AT^2\exp\left(-\frac{q\phi_B}{kT}\right)\exp\left(\frac{qV}{kT}\right) \qquad \text{Eq.5.4.}$$

where $A = 4\pi m^* k^2/h^3$ is the Richardson constant and ϕ_B is the barrier height. In the expression of the Richardson constant m^* is the effective mass of the charge carriers and h is the Planck constant.

The second theory is the so-called diffusion theory, where the driving force, which is distributed over the whole length of the depletion layer, is the difference in carrier concentration. Hence, the current is limited by diffusion (similarly to that of a bulk semiconductor or a p-n junction), rather than the barrier height and is given by[32]

$$J = qN_V D\left[\exp\left(\frac{qV}{kT}\right)-1\right] / \int_0^{W_D} \exp\left[\frac{E_V(x)}{kT}\right]dx \qquad \text{Eq.5.5.}$$

where N_V is the effective density of states in the valence band edge, D is the diffusion coefficient, W_D is the depletion width and E_V is the valence band edge. Assuming full depletion of our devices[33] and a triangularly shaped barrier, Eq. 5.5 can be modified and the current density can be expressed as

$$J = \frac{A\sqrt{T}\phi_B}{\exp\left(\frac{q\phi_B}{kT}\right)-1}\left[\exp\left(\frac{qV}{kT}\right)-1\right] \qquad \text{Eq.5.6.}$$

where $A=d^2N_VD/dk$.We used Eq. 5.4. and Eq. 5.6. to predict the values of J_0. The thermionic emission model predicts two orders of magnitude lower J_o at lower temperatures. Note that independently of the barrier height, the fit never agrees with the experimental data, since the slope of J_o does not change. However, the diffusion theory provides perfect agreement to the experimental data. These observations are consistent with previous reports on Schottky barriers in Al/PbS junctions[34] and other low mobility semiconductors[35]. Moreover, the fitting process of J_o allows the direct extraction of ϕ_B, and the diffusion coefficient (D), which can be used to calculate theoretical values of mobilities (μ) at different temperatures (Figure 5.4). The calculated value of the barrier height from Eq.5.6. is $\phi = 0.545\ eV$, which is in good agreement with previous experimental findings.[36,37]

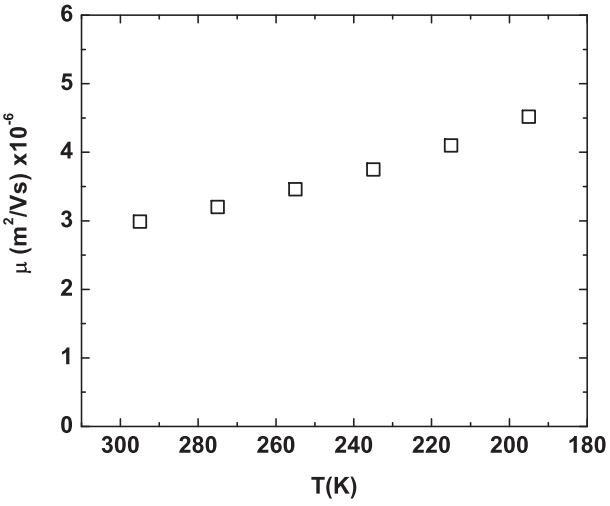

Figure 5.4 Temperature dependence of the predicted mobility, obtained from the Einstein-relation.

The theoretical mobility, which was calculated using the famous Einstein relation ($\mu=D/kT$), depends weakly on temperature, showing a slight increase with decreasing temperature. This behavior is in contradiction with a hopping based transport mechanism, since in that case the mobility should dramatically decrease with temperature.[19,38] However, if we consider that the active layer of our solar cells consists of clusters with varying degrees of coupling, the mobility can probably be explained as the superposition of band-like and hopping transport mechanism.

This idea is supported by low temperature measurements on BDT treated PbS NC thin films to be shown later in this chapter. However, it is still premature to draw a certain conclusions regarding the charge transport process in PbS NC solar cells due to contradictory reports and experimental data.

To evaluate the credibility of the obtained values for J_o, we used Eq. 5.2. to fit the experimental values of the V_{oc} at different temperatures. The measured and calculated V_{oc} at different temperatures are shown in Figure 5.5. Clearly, the calculated V_{oc} provides a very close match to the experimental data. Consequently, the temperature dependence of V_{oc} can be explained by the temperature dependence of J_o. As J_o decreases with temperature, V_{oc} starts to increase. Nevertheless, the exact reason for the dramatic decrease of the J_{sc} at lower temperatures still remains not fully explained.

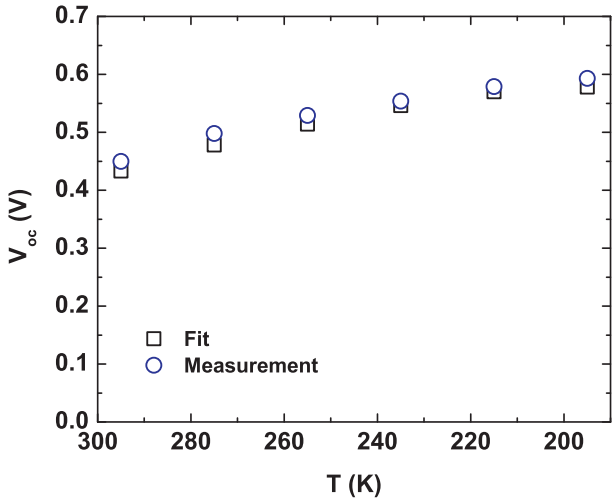

Figure 5.5 Experimental temperature dependence of the V_{oc} (○) in comparison with the calculated V_{oc}(□).

5.2.2 Temperature dependence of optical properties

Temperature dependent optical density

The temperature dependence of the optical density (OD) of oleic acid stabilized PbS NCs (o-PbS) has already been studied by other authors.[21,22] A typical experimental dataset of the temperature dependent OD of drop casted PbS NCs is shown in Figure 5.6 (a).

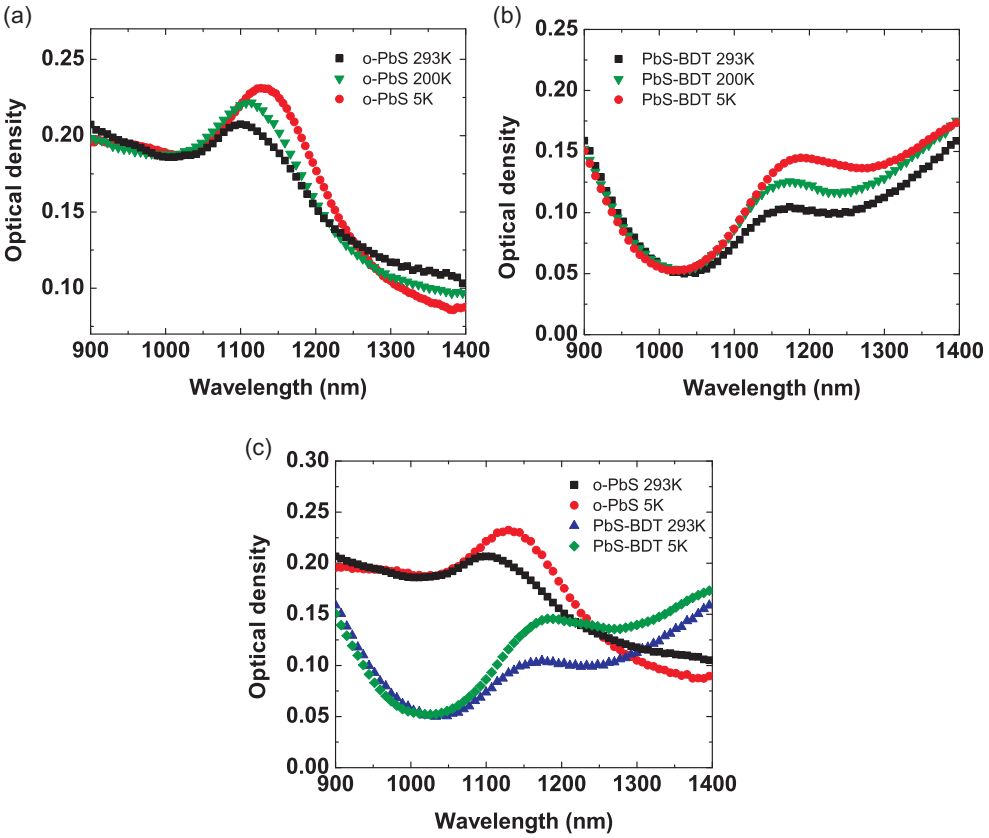

Figure 5.6 Temperature dependent absorption spectra of (a) PbS NCs with oleic acid ligands (b) PbS NCs cross-linked with BDT and (c) comparison of the absorption spectra before and after BDT treatment.

As can be seen, the first excitonic peak of the PbS NCs is located at ~1100 nm at 293K. With decreasing temperature the OD spectra shows a red-shift and the intensity of the first excitonic peak increases. At 5K the first excitonic peak is situated at ~ 1130 nm. This red-shift of the OD spectra entails the temperature

variation of the energy bandgap (E_g), namely that E_g decreases with decreasing temperature.

The temperature dependence of the E_g can be explained by considering the thermal expansion of the NCs bandgap with temperature. The measure of the degree of this expansion is dE_g/dT, which is called the temperature coefficient.[39] This coefficient depends strongly on the NC`s size. It has been shown that for PbS and PbSe NCs this coefficient decreases with decreasing NC size by more than an order of magnitude compared to the bulk values and it even becomes negative below diameters as small as 3 nm.[21] However, for PbS NCs with diameters as large as 7 nm, the coefficient was found to be very close to the bulk value. This shows that by decreasing the size of the NC, the temperature dependence gets weaker as it would be expected for atomic like levels.

The temperature coefficient at constant pressure (P) can be expressed as[28]

$$\left(\frac{\partial E_g}{\partial T}\right)_P = \left(\frac{\partial E_g}{\partial T}\right)_V - \left(\frac{\alpha}{\beta}\right)\left(\frac{\partial E_g}{\partial P}\right)_T \qquad \text{Eq. 5.7.}$$

where α and β are the volume coefficient of the thermal expansion and the volume compressibility, respectively. According to Eq. 5.7., the temperature dependence of the E_g is determined by two terms. The first term ($(\partial E_g/\partial T)_V$) originates from the change of the electron-phonon interaction with temperature, while the second term ($(\alpha/\beta)(\partial E_g/\partial P)_T$) comes from the lattice constant variation with temperature. Using experimental results for α and β, the temperature coefficient is positive since both the ($(\partial E_g/\partial T)_V$ and [$-(\alpha/\beta)(\partial E_g/\partial P)_T$] are positive.[28] Consequently, the increase of the temperature leads to the increase of the bandgap.

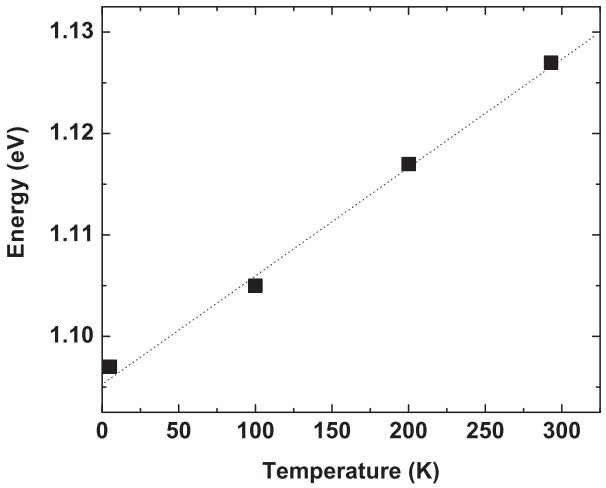

Figure 5.7 Temperature dependence of the energy gap of o-PbS NCs.

To obtain dE_g/dT, E_g was estimated in units of eV from the OD spectra at different temperatures and plotted in Figure 5.7. The value of dE_g/dT was determined from the linear fit and calculated to be 104 μeV/K; which means that the bandgap of the NCs increases 104 μeV per 1K. This extracted value is very close to the values reported in the literature.[21]

Figure 5.6 (b) shows the OD spectra of PbS NCs after cross-linking with BDT molecules (PbS-BDT) at different temperatures. The first excitonic peak at 293K is located at ~ 1170 nm and is red-shifted by ~15 nm at 5K. At this temperature the oscillator strength of the excitonic transition increases due to the less electron-phonon interaction. In addition, a broad band appears from ~ 1280 nm and onwards, which can be attributed either to the wave function overlaps and/or to the appearance of defect states as a result of the cross-linking process. Drude-type absorption[40] also could be the reason for the spectral broadening; this could eventually be ruled out by measuring the optical density further down to the infrared. Note, that this broadening cannot be observed on the IPCE spectra (Figure 4.5. (b)), indicating that the absorption from this region does not contribute to the photocurrent. This agrees with the presence of defect states on the NCs` surface. The broadening of the spectra above the first excitonic peak after EDT treatment was illustrated in several studies, however, without any comment on the underlying physical reason.[4,20]

The comparison at 293K and 5K between the OD of o-PbS and PbS-BDT is illustrated in Figure 5.6 (c). At 293K, the first excitonic peak of PbS NCs remains, but is red-shifted by 70 nm after BDT treatment (from 1100 nm to 1170 nm) and by 55 nm at 5 K. Moreover, the peak is broadened and has decreased in intensity with respect to the NCs stabilized by oleic acid ligands, which is again the result of the surface modification. When PbS NCs are stabilized by oleic acid ligands, the electron and hole wave functions are localized on the individual NCs, while after BDT treatment the NCs are pulled closer together, and most probably the result is a mixture where some of the wave functions remain localized, but some start to couple, relaxing the quantum confinement.[1] As a consequence, the excitons become delocalized over several NCs. The additional red-shift of the OD of PbS-BDT with decreasing temperature can be explained by the thermal expansion, as has been demonstrated above.

The coupling between the energy levels of NCs can be characterized by the so-called coupling energy $\beta \approx h\Gamma$, where h is the Planck constant and Γ is the tunneling rate.[1,41] The tunneling rate is in direct correlation with the separation distance between individual NCs. If β is smaller than the thermal energy kT, the coupling is very weak and the charge transport can only occur by sequential tunneling between the NCs. However, if β is larger than kT, the NCs are strongly coupled, the discrete wave functions start to overlap and above a transition point

form molecular-like orbitals extended over several NCs.[1] For optoelectronics, the ultimate goal would be to design NCs with strong coupling but maintaining a certain amount of optical confinement, which would result in bulk-like transport properties.

Since the first excitonic peak is still present together with spectral broadening on the OD spectra of PbS-BDT NC thin films, we propose that the device active layer is indeed composed of inhomogenously coupled NCs and this leads to complex charge transport mechanisms (including hopping/tunneling and band-like transport).[42]

Temperature dependent steady state photoluminescence (PL)

Similarly to the absorption, the PL spectra of o-PbS NCs and PbS-BDT exhibit a strong temperature dependence as well. The experimental dataset of the steady-state PL spectra of the o-PbS NCs thin films at different temperatures is presented in Figure 5.8 (a).

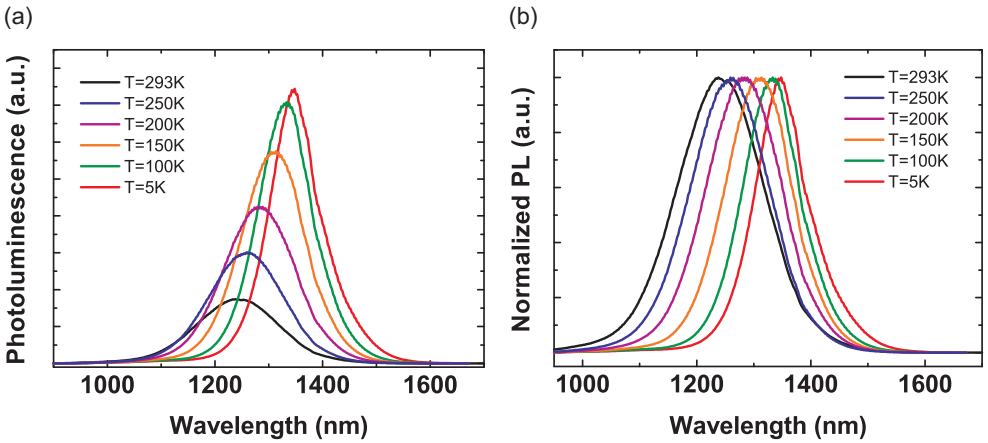

Figure 5.8 Steady-state (a), and normalized PL (b) spectra of o-PbS NCs.

The PL of o-PbS NCs at 293 K shows a maximum at 1242 nm and a red-shift to 1346 nm with decreasing temperature. In addition to the red-shift, the full width at half maximum (FWHM) of the PL spectra decreases to 46 % of its original value. (The PL maxima and FWHM values were determined from Gaussian fits of the PL spectra at different temperatures.) Moreover, the PL intensity increases with decreasing temperature by more than a factor of 4.

The red-shift can be explained by the thermal expansion discussed above. Due to this phenomenon, the temperature decrease leads to the reduction of the energy band gap. The decrease of the FWHM and the increase in the PL intensity with decreasing temperature is due to the suppression of the phonon-coupled quenching of the excitons. In detail, the probability of the electron-phonon scattering

decreases due to the reduced number of lattice vibrations (phonons) at lower temperatures. As a result, the magnitude of nonradiative losses is decreased and the PL is enhanced. These considerations are in agreement with previous reports on temperature dependence studies of NCs` PL.[23,26]

In contrast, after surface modification of o-PbS NCs with BDT molecules, the PL of the NCs becomes more complex and shows peculiar properties. The PL of PbS-BDT at 293K shifts to the red and the intensity of the PL is quenched with respect to the PL of o-PbS NCs, as illustrated in Figure 5.9 (a). By decreasing the temperature, additional red-shift occurs (Figure 5.9 (b)), similarly to the PL of o-PbS NCs, which can also be explained by the thermal expansion phenomenon.

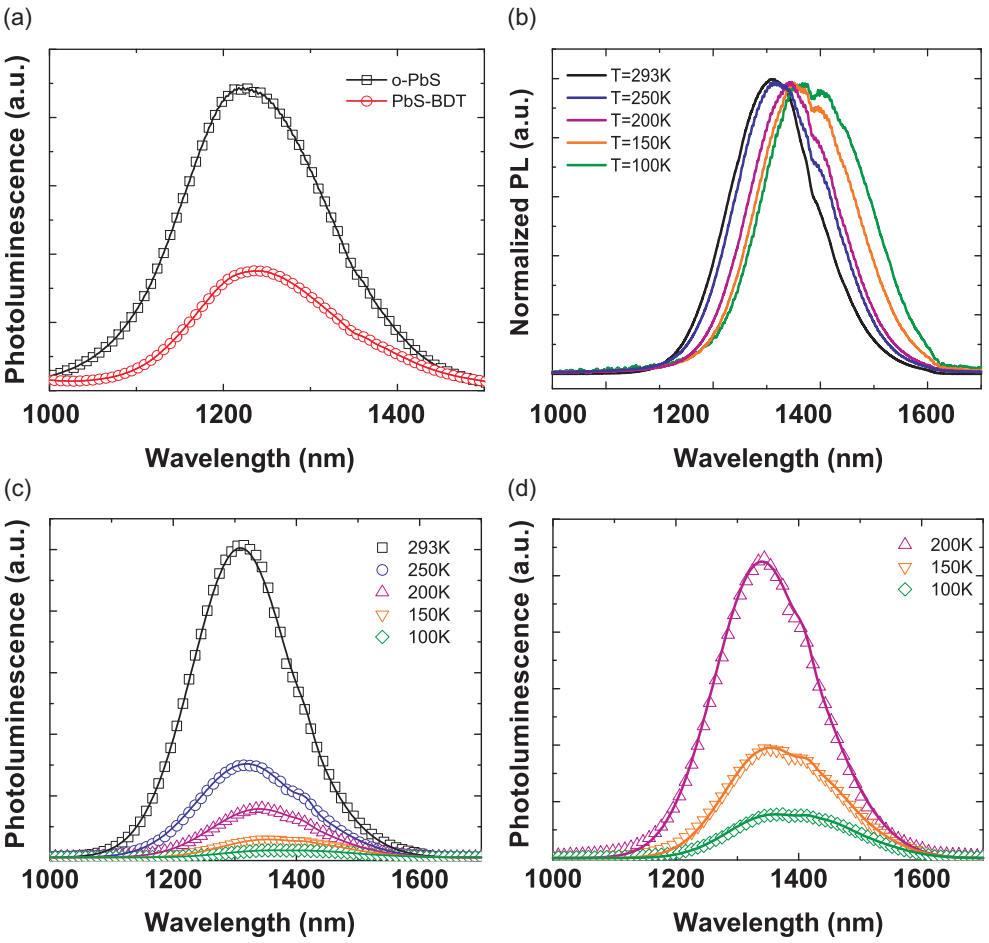

Figure 5.9 (a) Steady-state PL spectra of the o-PbS NCs and PbS-BDT at 293K; (b) Red shift of the normalized steady state PL of PbS-BDT with decreasing temperature; (c)-(d) Gaussian fits of the steady state PL of PbS-BDT at different temperatures.

However, instead of the PL enhancement, we observed PL quenching at lower temperatures as well as the appearance of additional peaks on the higher wavelength side of the excitonic emission. This indicates that at lower temperatures nonradiative processes come into play through defect states, causing the loss of the PL intensity and the appearance of extra peaks. It is unexpected to increase the PL with increasing temperature, where the electron-phonon interactions become more important. There are strikingly few reports discussing the temperature anti-quenching of the PL. Wuister *et al.* investigated the temperature anti-quenching of PL in CdSe and CdTe NCs and indicated that the surface passivation decreases with temperature due to the phase transition of the capping ligands and displacements of the surface atoms.[43,44]

The role of the coordinating ligands around the NCs concerns not only the stabilization in solution and confinement of the charge carriers inside the NCs, but also the passivation of the dangling lone electron pairs of the surface atoms (Pb and S).The modification of the NCs` surface has a large effect on their optical properties. It has been demonstrated that the spatial confinement is very sensitive to surface-ligand interaction and subtle changes in the nature of the stabilizing ligands can increase or decrease the PL quantum efficiency.[7,45-47] Insufficient passivation of the NCs` surface leads to the appearance of defect states, which can create radiative and nonradiative pathways for recombination of the charge carriers upon excitation.[46-49] For instance, Pendyala and co-workers suggested that the Pb dangling bonds form shallow donor states close to the conduction band edge, while dangling bonds of S atoms can create acceptor states in the middle of the bandgap of PbS NCs.[50] Bryant and Jaskolski reported similar observations on passivated and unpassivated CdS NCs.[51] In addition, as was mentioned before, if the distance between adjacent NCs decreases, the confinement of charge carriers relaxes which could also cause a decrease of the PL. To sum up, due to relaxation of the quantum confinement and the reduction of surface passivation the excitonic emission of the NCs can be quenched and the spectral shape can be modified due to emerging transitions, originating from new states located in the NCs`bandgap. Note, that the main dip ~1380 nm (Figure 5.9) could be due to the absorption of water being present in the optical path; however, the PL measurements were performed in vacuum and the PbS-OA samples measured under the same conditions did not show similar features.

Since the shape of the PL after surface modification is rather complicated, it is difficult to draw conclusions without further analysis. To gain deeper insight into our experimental results, the PL spectra of PbS-BDT at different temperatures were fitted by using 4 Gaussian curves. The sum of the 4 Gaussians provides a good fit to the experimental data as shown in Figure 5.9 (c) and (d). The parameters extracted from the Gaussian analysis are illustrated in Figure 5.10.

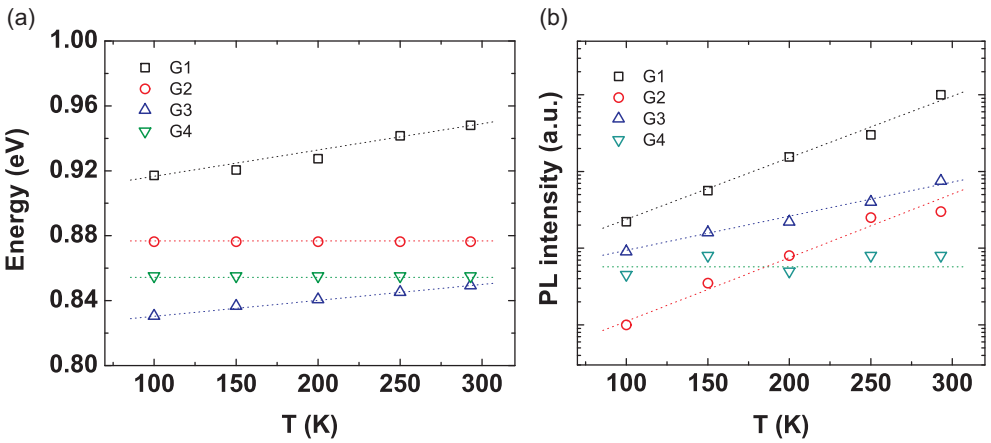

Figure 5.10 Temperature dependence of the (a) PL peak energy and (b) peak intensity as obtained from the Gaussian fits (Figure 5.9 (c-d))

Figure 5.10 (a) shows the temperature dependence of the Gaussian peak energy. Gaussian 1 (G1) is attributed to the excitonic emission while G2-4 can be related to defect and impurity-associated transitions. It is interesting to note that G3 shows a similar trend to G1 with decreasing temperature, suggesting the intrinsic origin of this state and/or a strict correlation with the excitonic peak. However, the presence of this state is not evidenced in the o-PbS samples which could be due to the fact that the emission intensity of o-PbS is much stronger than the one of PbS-BDT, covering the emission from this intrinsic defect related state. In contrary, G2 and G4 do not show any shift in peak position by decreasing the temperature. These emissions can be attributed to surface defects introduced by the surface modification.

Figure 5.10 (b) illustrates how the PL intensity of the 4 Gaussians changes with temperature. As can be seen, G4 does not change in intensity, while G1-3 are all quenched by decreasing the temperature. The quenching mechanism appears to be mediated by defect states, but further investigations are required to reveal the underlying processes. However, we can safely conclude that due to the presence of surface defects, new radiative and nonradiative pathways compete with the excitonic emission. The overall effect is to decrease the total PL while the ratio between the relative intensity of the excitonic PL and the defect related emissions (G3 and G4) decreases. The decrease of the excitonic emission with decreasing temperature cannot be explained purely by the depopulation through defect states, since in that case the relative intensity of the emission from the defect related states should increase (see further on). In contrast, the emission from these states decreases, therefore the opening of non-radiative pathways in combination with defect-associated transitions could explain the experimental results. We propose a PbS band diagram in Figure 5.11, illustrating all possible pathways for the radiative

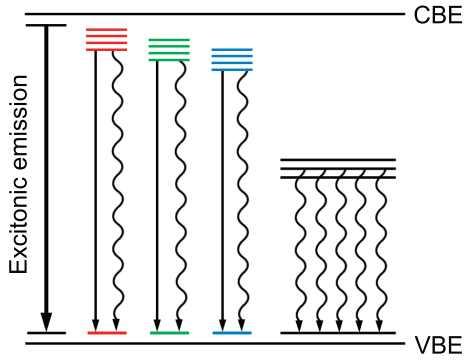

Figure 5.11 Schematic of the radiative and nonradiative pathways in PbS-BDT. CBE and VBE symbolize the conduction and valence band edge, respectively. The red, green and blue lines represent the defect states originating from impurity and Pb dangling bonds. The midgap states created due to S dangling bonds are illustrated by black lines.

(straight black arrows) and nonradiative transitions (sinoidal black arrows). We suggest that G2-4 originate from impurity and Pb dangling bond induced defect states while S dangling bonds introduce midgap states serving as nonradiative quenching centers.

Charge carrier losses through defect related states could also explain the decrease of J_{sc} with decreasing temperature. Future time-resolved PL experiments could provide more information to understand the quenching mechanisms in PbS-BDT samples.

Temperature dependent time-resolved photoluminescence

The study of the PL dynamics can provide additional information on the recombination of the photoinduced excitations. Figure 5.12 (a) and (b) illustrate the PL decay at 293K before and after surface modification, respectively. The PL decay of o-PbS NCs shows a mono-exponential decay with a time constant of ~ 35 ns, while after BDT treatment the PL decay becomes bi-exponential with a slower component of ~ 2.5 ns and a faster component of ~ 203 ps. The reduction of the PL lifetime strongly suggests the presence of nonradiative processes. The bi-exponential behavior and the shorter lifetime can be attributed to several phenomena: i) a transfer of the excitation to the defect states, depopulating the excitonic level; ii) the coexistence of regions with and without partial relaxation of the quantum confinement. Unfortunately, due to the strong red-shift and the decrease in intensity, we were not able to measure the decay time at lower temperatures. To displace the low temperature photoluminescence from the edge of the spectral response of our instrument we used NCs with diameters of ~ 3.4 nm. However, even with these smaller NCs we were only able to measure the low temperature PL decay of o-PbS NCs, since the signal from PbS-BDT was too weak due to the large quenching.

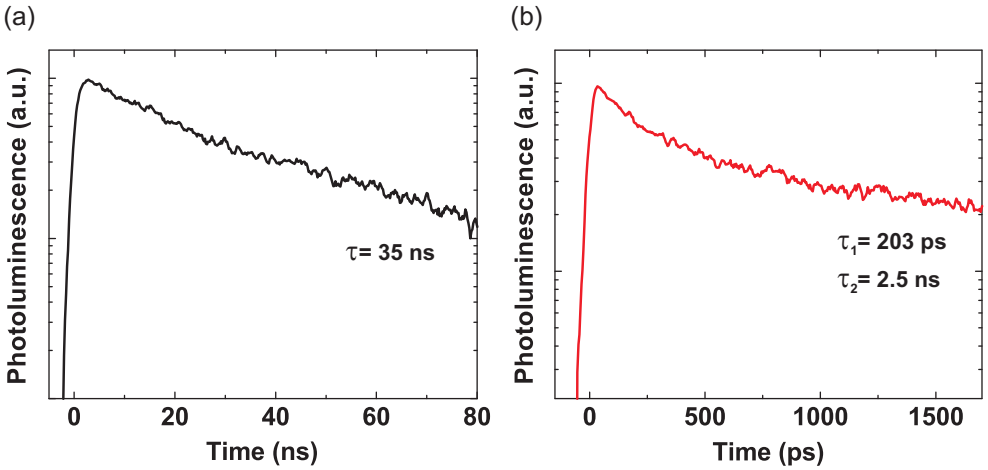

Figure 5.12 PL decay of (a) o-PbS and (b) PbS-BDT at 293K.

The decay of the PL of o-PbS NCs is reported in Figure 5.13. The dashed black lines represent the exponential fits used to determine the decay time at different temperatures. The PL decay is mono-exponential and it becomes slower with decreasing temperature. The PL decay time is calculated to be ~0.6 μs at 293K while at 5K the decay time is increased to 5.4 μs.

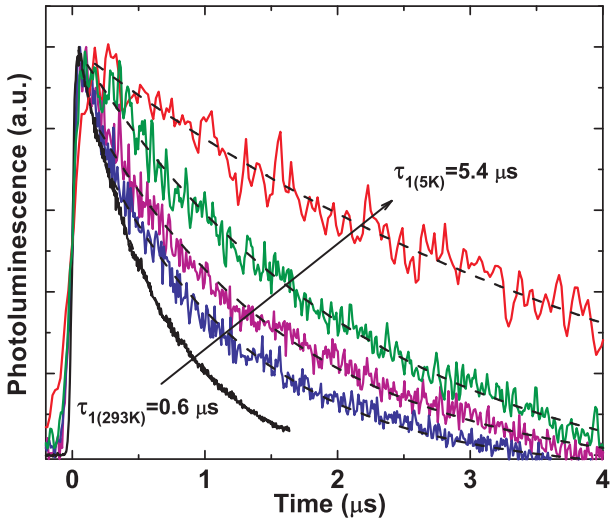

Figure 5.13 Temperature dependence of the PL decay of o-PbS NCs with diameter of ~ 3.4 nm and PL maximum at ~ 1060 nm.

This temperature dependence of the decay time can be explained as mentioned previously by the suppression of the phonon-coupled quenching of the excitons. By

decreasing the temperature, the magnitude of the lattice vibration decreases, resulting in reduced scattering.

5.3 Conclusions

We sought to explain the temperature dependence of PbS NC solar cells. We have demonstrated that the overall effect of the temperature on the device efficiency originates from the temperature dependence of V_{oc} and J_{sc}. The net effect is that the V_{oc} increases and J_{sc} decreases with decreasing temperature, while the *FF* remains approximately constant. The temperature dependence of the V_{oc} of the PbS solar cells was successfully modeled by using the extracted values of the J_0 at different temperatures. The thermionic emission model predicted two orders of magnitude lower J_o at lower temperatures than the diffusion theory, which provided perfect agreement to the experimental data.

The optical density (OD) of o-PbS films is red-shifted when the temperature is reduced from 293K due to the temperature variation of the energy bandgap, namely that E_g decreases with the temperature. The temperature dependence of the energy gap can be explained by considering the thermal expansion of the NCs`bandgap with temperature. After BDT treatment, the first excitonic peak is red-shifted with respect to the absorption of o-PbS films and a broad band appears from ~ 1280 nm and onwards, which can be attributed either to the wave function overlaps and/or to the appearance of defect states as a result of the cross-linking process.

Since the first excitonic peak is still present together with spectral broadening of the OD spectra of PbS-BDT NC thin films, we propose that the device active layer is composed of inhomogenously coupled NCs, which could lead to complex charge transport mechanisms including hopping/tunneling and band-like transport.

Similarly to the absorption, the PL spectra of o-PbS NCs and PbS-BDT exhibit a strong temperature dependence as well. The PL of o-PbS NCs is red-shifted and the FWHM of the PL spectra decreased to 46 % of its original value. In contrast, the PL of PbS-BDT becomes more complex besides showing a red-shift. Instead of the enhancement of the PL, the cross-linked NCs exhibit quenched PL at lower temperatures and additional peaks appear on the higher wavelength side of the excitonic emission. The quenching indicates the presence of nonradiative pathways at lower temperatures which can be ascribed to defect states. This is supported by an analysis of the PL spectra of the PbS-BDT at different temperatures, based on fitting Gaussian curves to the experimental data. The analysis suggests the appearance of intrinsic and surface related defect states which could serve as radiative and nonradiative channels for recombination of the charge carriers.

The comparison of the PL decay of o-PbS NCs and PbS-BDT also indicates the presence of nonradiative processes. The shorter lifetime of the PL decay of PbS-BDT films can be attributed to the transfer of the excitation from the excitonic level to the defect states.

5.4 Experimental

For low temperature *J-V* measurements PbS NC solar cells were prepared as mentioned in the experimental part of Chapter 4. Current-voltage characteristics were recorded at different temperatures using a Keithley 2400 SourceMeter in a nitrogen filled glove-box. The desired temperatures were obtained by cooling with liquid nitrogen. Measurements were performed in the dark and under illumination from a Steuernagel SolarConstant 1200 metal halide lamp calibrated to 1 sun intensity and corrected for spectral mismatch with the AM1.5G spectrum using a Si reference cell.

Low temperature optical density measurements were performed by using an absorption setup consisting of a Tungsten lamp, a liquid helium cooled continuous flow (He-flux) Oxford Optistat cryostat, a monochromator and an Andor InGaAs photodiode array detector.

For low temperature steady state and time-resolved PL measurements, the samples were prepared on quartz substrates and loaded into the same He-flux cryostat. The samples were excited at ~380 nm by the second harmonic of a mode-locked Ti:Sapphire laser delivering pulses of 150 fs. To vary the repetition frequency of the exciting pulse an optical pulse selector was used. Time-resolved traces were recorded with a Hamamatsu streak camera working in single sweep mode. The steady-state PL spectra in the near-infrared were obtained with an InGaAs detector from Andor. The PL spectra were corrected for the spectral response of the setup.

References

(1) Talapin, D. V.; Lee, J.-S.; Kovalenko, M. V.; Shevchenko, E. V. *Chem. Rev.* **2010**, *110*, 389-458.

(2) Sargent, E. H. *Adv. Mater.* **2008**, *20*, 3958-3964.

(3) Tang, J.; Wang, X.; Brzozowski, L.; Barkhouse, D. A. R.; Debnath, R.; Levina, L.; Sargent, E. H. *Adv. Mater.* **2010**, *22*, 1398-1402.

(4) Luther, J. M.; Law, M.; Beard, M. C.; Song, Q.; Reese, M. O.; Ellingson, R. J.; Nozik, A. J. *Nano Lett.* **2008**, *8*, 3488-3492.

(5) Moreels, I.; Lambert, K.; Smeets, D.; De Muynck, D.; Nollet, T.; Martins, J. C.; Vanhaecke, F.; Vantomme, A.; Delerue, C.; Allan, G.; Hens, Z. *ACS Nano* **2009**, *3*, 3023-3030.

(6) Cho, K.-S.; Talapin, D. V.; Gaschler, W.; Murray, C. B. *J. Am. Chem. Soc.* **2005**, *127*, 7140-7147.

(7) Hanrath, T.; Veldman, D.; Choi, J. J.; Christova, C. G.; Wienk, M. M.; Janssen, R. A. J. *ACS Appl. Mater. Interfaces* **2009**, *1*, 244-250.

(8) Kuo, C.-Y.; Su, M.-S.; Ku, C.-S.; Wang, S.-M.; Lee, H.-Y.; Wei, K.-H. *J. Mater. Chem.* **2011**.

(9) Talapin, D. V.; Murray, C. B. *Science* **2005**, *310*, 86 -89.

(10) Luther, J. M.; Law, M.; Song, Q.; Perkins, C. L.; Beard, M. C.; Nozik, A. J. *ACS Nano* **2008**, *2*, 271-280.

(11) Liu, Y.; Gibbs, M.; Puthussery, J.; Gaik, S.; Ihly, R.; Hillhouse, H. W.; Law, M. *Nano Lett.* **2010**, *10*, 1960-1969.

(12) Zarghami, M. H.; Liu, Y.; Gibbs, M.; Gebremichael, E.; Webster, C.; Law, M. *ACS Nano* **2010**, *4*, 2475-2485.

(13) Talapin, D. V.; Murray, C. B. *Science* **2005**, *310*, 86-89.

(14) Law, M.; Luther, J. M.; Song, Q.; Hughes, B. K.; Perkins, C. L.; Nozik, A. J. *J. Am. Chem. Soc.* **2008**, *130*, 5974-5985.

(15) Tsang, S. W.; Fu, H.; Wang, R.; Lu, J.; Yu, K.; Tao, Y. *Appl. Phys. Lett.* **2009**, *95*, 183505.

(16) Choi, J. J.; Luria, J.; Hyun, B.-R.; Bartnik, A. C.; Sun, L.; Lim, Y.-F.; Marohn, J. A.; Wise, F. W.; Hanrath, T. *Nano Lett.* **2010**, *10*, 1805-1811.

(17) Klem, E. J. D.; MacNeil, D. D.; Cyr, P. W.; Levina, L.; Sargent, E. H. *Appl. Phys. Lett.* **2007**, *90*, 183113.

(18) Zarghami, M. H.; Liu, Y.; Gibbs, M.; Gebremichael, E.; Webster, C.; Law, M. *ACS Nano* **2010**, *4*, 2475-2485.

(19) Kang, M. S.; Sahu, A.; Norris, D. J.; Frisbie, C. D. *Nano Lett.* **2010**, *10*, 3727-3732.

(20) Tang, J.; Brzozowski, L.; Barkhouse, D. A. R.; Wang, X.; Debnath, R.; Wolowiec, R.; Palmiano, E.; Levina, L.; Pattantyus-Abraham, A. G.; Jamakosmanovic, D.; Sargent, E. H. *ACS Nano* **2010**, *4*, 869-878.
(21) Olkhovets, A.; Hsu, R.-C.; Lipovskii, A.; Wise, F. W. *Phys. Rev. Lett.* **1998**, *81*, 3539.
(22) Kim, D.; Kuwabara, T.; Nakayama, M. *J. Lumin.* **2006**, *119-120*, 214-218.
(23) Rinnerbauer, V.; Egelhaaf, H.-J.; Hingerl, K.; Zimmer, P.; Werner, S.; Warming, T.; Hoffmann, A.; Kovalenko, M.; Heiss, W.; Hesser, G.; Schaffler, F. *Phys. Rev. B* **2008**, *77*, 085322.
(24) Lü, W.; Kamiya, I.; Ichida, M.; Ando, H. *Appl. Phys. Lett.* **2009**, *95*, 083102.
(25) Liu, C.; Kwon, Y. K.; Heo, J. *J. Non-Cryst. Solids* **2009**, *355*, 1880-1883.
(26) Gaponenko, M. S.; Lutich, A. A.; Tolstik, N. A.; Onushchenko, A. A.; Malyarevich, A. M.; Petrov, E. P.; Yumashev, K. V. *Phys. Rev. B* **2010**, *82*, 125320.
(27) Pichler, S.; Rauch, T.; Seyrkammer, R.; Böberl, M.; Tedde, S. F.; Fürst, J.; Kovalenko, M. V.; Lemmer, U.; Hayden, O.; Heiss, W. *Appl. Phys. Lett.* **2011**, *98*, 053304.
(28) Dalven, R. In *Advances in Research and Applications*; Academic Press, 1974; Vol. Volume 28, pp. 179-224.
(29) Sriprapha, K.; Yunaz, I. A.; Myong, S. Y.; Yamada, A.; Konagai, M. *Jpn. J. Appl. Phys.* **2007**, *46*, 7212-7216.
(30) Katz, E. A.; Faiman, D.; Tuladhar, S. M.; Kroon, J. M.; Wienk, M. M.; Fromherz, T.; Padinger, F.; Brabec, C. J.; Sariciftci, N. S. *J. Appl. Phys.* **2001**, *90*, 5343.
(31) Bagienski, W.; Gupta, M. C. *Sol. Energy Mater. Sol. Cells* **2011**, *95*, 933-941.
(32) Sze, S. M.; Ng, K. K. *Physics of Semiconductor Devices*; John Wiley & Sons, Inc.: Hoboken, NJ, USA, 2006.
(33) Luther, J. M.; Law, M.; Beard, M. C.; Song, Q.; Reese, M. O.; Ellingson, R. J.; Nozik, A. J. *Nano Lett.* **2008**, *8*, 3488-3492.
(34) Clifford, J. P.; Johnston, K. W.; Levina, L.; Sargent, E. H. *Appl. Phys. Lett.* **2007**, *91*, 253117.
(35) Assadi, A.; Svensson, C.; Willander, M.; Inganäs, O. *J. Appl. Phys.* **1992**, *72*, 2900.
(36) Konstantatos, G.; Sargent, E. H. *Appl. Phys. Lett.* **2007**, *91*, 173505.
(37) Gao, J.; Luther, J. M.; Semonin, O. E.; Ellingson, R. J.; Nozik, A. J.; Beard, M. C. *Nano Lett.* **2011**, *11*, 1002-1008.
(38) Craciun, N. I.; Wildeman, J.; Blom, P. W. M. *Phys. Rev. Lett.* **2008**, *100*, 056601.

(39) Nalwa, H. S. *Handbook of thin film materials: Nanomaterials and magnetic thin films*; Academic Press, 2002.
(40) Tamura, K.; Hirakawa, K.; Shimada, Y. *Physica B* **1999**, *272*, 183-186.
(41) Liu, Y.; Gibbs, M.; Puthussery, J.; Gaik, S.; Ihly, R.; Hillhouse, H. W.; Law, M. *Nano Lett.* **2010**, *10*, 1960-1969.
(42) Markovich, G.; Collier, C. P.; Henrichs, S. E.; Remacle, F.; Levine, R. D.; Heath, J. R. *Acc. Chem. Res.* **1999**, *32*, 415-423.
(43) Wuister, S. F.; van Houselt, A.; de Mello Donegá, C.; Vanmaekelbergh, D.; Meijerink, A. *Angew. Chem. Int. Ed.* **2004**, *43*, 3029-3033.
(44) Wuister, S. F.; de Mello Donegá, C.; Meijerink, A. *J. Am. Chem. Soc.* **2004**, *126*, 10397-10402.
(45) Talapin, D. V.; Rogach, A. L.; Kornowski, A.; Haase, M.; Weller, H. *Nano Lett.* **2001**, *1*, 207-211.
(46) Kuno, M.; Lee, J. K.; Dabbousi, B. O.; Mikulec, F. V.; Bawendi, M. G. *J. Chem. Phys.* **1997**, *106*, 9869.
(47) de Mello Donegá, C.; Hickey, S. G.; Wuister, S. F.; Vanmaekelbergh, D.; Meijerink, A. *J. Phys. Chem. B* **2003**, *107*, 489-496.
(48) Kapitonov, A. M.; Stupak, A. P.; Gaponenko, S. V.; Petrov, E. P.; Rogach, A. L.; Eychmüller, A. *J. Phys. Chem. B* **1999**, *103*, 10109-10113.
(49) Nonoguchi, Y.; Nakashima, T.; Kawai, T. *J.Phys.Chem.C* **2007**, *111*, 11811-11815.
(50) Pendyala, N. B.; Koteswara Rao, K. S. R. *J. Lumin.* **2008**, *128*, 1826-1830.
(51) Bryant, G. W.; Jaskolski, W. *J. Phys. Chem. B* **2005**, *109*, 19650-19656.